CHAPTER 17

COVID-19 Boon or Bane: A case study of Air pollutant transport in the Yangtze River Delta region and its consequent health effects during the COVID-19 lockdown period

Li Li[a], Qing Li[a], Ling Huang[a], Elly Arukulem Yaluk[a], Yangjun Wang[a], Qian Wang[a], Ansheng Zhu[a], Jian Xu[a], Ziyi Liu[a], Hongli Li[a], Lishu Shi[a], Yonghui Zhu[a], Andy Chan[b]

[a]School of Environmental and Chemical Engineering, Shanghai University, Shanghai, China
[b]Department of Civil Engineering, University of Nottingham Malaysia, Semenyih, Selangor, Malaysia

17.1 Introduction

The tragic outbreak of COVID-19 pandemic during 2020 (Tian et al., 2020; Wang et al., 2020a) has caused tremendous impacts on people's livelihoods across the world (Wang et al., 2020a). To date (as of 12th, December 2020), there have been 69,808,588 confirmed cases of COVID-19, including 1,588,854 deaths globally according to World Health Organization (WHO; https://covid19.who.int). From the time when the pandemic started, the government of the People's Republic of China rolled-out rigorous response policies to control the rapid spread of the disease (Tian et al., 2020; Wang et al., 2020b). This included shutting down of education institutions, industrial operations, construction activities and restaurants; restriction of traffic and reduction in the number of vehicle kilometres travelled (VKT); cancellation of mass gatherings and events; and enforcement of social distancing and personal protection. Ultimately, the spread of the disease was brought under control. Besides, the air quality during the lockdown period improved significantly in China as a result of reduced industrial activities. Notably, the concentrations of $PM_{2.5}$, NO_2 and other key pollutants were reduced substantially in the designated key regions of China based on evidences from satellite imagery and ground-based measurements (NASA, 2020; Wang et al., 2020a, 2020b).

The Yangtze River Delta (YRD) region is one of the major economic city-clusters in China. Usually, the wintertime pollution episodes in the YRD region raises a lot of attention, attributed mainly to unfavourable meteorological conditions (Huang et al., 2019; Li et al., 2018, 2019). In early 2020 coincidentally, the lowered human activities during the COVID-19 lockdown in YRD occurred during the winter period. This presented

COVID-19 in the Environment
DOI: https://doi.org/10.1016/B978-0-323-90272-4.00010-5

an opportunity for comprehensive investigation of the level of air quality improvement attributable to different aspects of human activities and the corresponding health impact benefits. Typically, the COVID-19 control in the YRD followed the 'National Emergency Response Plan for Public Emergencies' issued by the Chinese government: Level I (particularly serious), Level II (serious), Level III (heavy) and Level IV (general). Therefore, this work studies the air quality and its transport during pre-lockdown period (before 24th January 2020); Level I response period (24th January to 25th February 2020) and Level II response period (26th February to 31st March 2020).

The pre-lockdown period was characterised by a "status-quo" for all socio-economic activities running normally and smoothly relative to similar periods in the previous years. However, from the 24th January 2020, abrupt halting of large-scale economic and social activities happened as Level I emergency response measures were affected. After about a month, gradual resumption to normalcy through Level II and Level III was instigated and observed. In a nutshell, the lockdown period (Level I and Level II) saw significant reduction or closure of transportation services, industrial enterprises, construction sites and catering enterprises among others.

It must be noted that each province in the YRD region implemented (and adjusted slightly differently) the COVID-19 response measures independently: the adjustments are based on variation of daily new confirmed cases and the number of people being cured and discharged from hospitals for each respective province. For instance, as the pandemic situation improved, Anhui and Jiangsu provinces downgraded its respective emergency response level to a secondary response on 25th February 2020. A week later, Zhejiang province also shifted to Level II on second March, while Shanghai adjusted to Level II three weeks later on 24th March. During the secondary response period, the cities in YRD under the premise of good protective measures, allowed some key industrial enterprises and construction sites to be operational with strict adherence to protective measures. Moreover, Level II response saw the blanket lifting and cancellation of the village closures, mandatory use of the public health QR-code for local travel, mandatory wearing of face mask as well as gradual relaxation and increase in road traffic. Most of the YRD region ultimately entered into Level III response since 31st March, with most activities gradually entering into operation (except schools and a few other sectors) with strict observation of protection measures.

The robust adjustment of socio-economic activities during the COVID-19 prevention and control period prompted a comprehensive assessment of the impact of reduced human activity on air pollution reduction. With this in end, an integrated approach is adopted to study the analysis of multi-pollutant observations, backward trajectory and potential source contribution analyses, estimates of pollutant emission reductions, and photochemical model simulations (Chang et al., 1987). The aim is to conduct a comprehensive assessment of the impact of reduced human activity on air pollution reduction. Along this direction of travel, the correlation between the substantial change of human and industrial activities on the air pollution scenarios in YRD during pre-lockdown,

Level I and Level II can be studied in depth. In addition, the changes of the source contributions as well as the sources of residual pollution related to local activity factors during the COVID-19 period can be better investigated.

The value for this study has clear policy implications for future air pollution control, but also provide invaluable information for health-related impact studies. The simulated results are here used to quantify the short-term health impacts by estimating the number of avoided premature death due to lowered $PM_{2.5}$ concentrations during COVID-19 lockdown.

17.2 Materials and methods

The hourly ambient concentrations of criteria air pollutants (SO_2, NO_2, CO, O_3, $PM_{2.5}$ and PM_{10}) are obtained publicly from the Ministry of Ecology and Environment of the People's Republic of China (http://datacenter.mep.gov.cn). In addition, meteorological data are obtained from the National Oceanic and Atmospheric Administration (NOAA)'s National Climate Data Centre archive (http://www.ncdc.noaa.gov/oa/ncdc.html) and also from the National Data Centre of the Chinese Meteorology Agency (http://data.cma.cn/).

17.2.1 Meteorological assessment during COVID-19

The Weather Research Forecasting model (WRF) version 3.4 (https://www.mmm.ucar.edu/wrf-model-general) is used to study the meteorological conditions during the COVID-19 period. Initial and boundary conditions (IC/BCs) for the WRF modelling are based on 1° × 1° grids FNL Operational Global Analysis data that are archived at the Global Data Assimilation System (GDAS). The BCs are updated at 6-hour intervals for the outmost domain. In addition, the Yonsei University (YSU) scheme (Hong et al., 2006) is applied to parameterise the boundary layer processes; the NOAH land surface scheme (Hong et al., 2006) is used to describe the land-atmosphere interactions; the Purdue-Lin microphysics scheme (Lin et al., 1983) is chosen to reproduce the cloud and precipitation processes; and the RRTM long-wave and Goddard Short-wave radiation schemes (Chou et al., 1999; Mlawer et al., 1997) are adopted to reflect the radiation. Parameterisation of the WRF model is listed in Table 17.1.

Table 17.1 Parameterization of the WRF model.

Item	Selection	Reference
Microphysics scheme	Purdue-Lin	Lin et al. (1983)
Short wave scheme	Goddard	Chou et al. (1999)
Long wave scheme	RRTM	Mlawer et al. (1997)
Planet boundary scheme	YSU scheme	Hong et al. (2006)
Cumulus scheme	Kain-Fritsch	Kain et al. (1993)
Land surface scheme	Noah land-surface	Ek et al. (2003)

17.2.2 Model set up and configuration

The WRF-CAMx model system is used to evaluate the improvement in air quality resulting from the reductions of human activities in the YRD region during COVID-19. WRF model provides the meteorology inputs for the simulations, while gridded hourly pollutant concentrations are generated by CAMx model Version 6.1 (http://www.camx.com/). The CAMx model is configured with CB06 (Yarwood et al., 2010), CF module and an updated mechanism of the Regional Acid Deposition Model (RADM) for the gaseous, aerosol and aqueous-phase processes respectively. The WRF-CAMx modeling domain is based on a Lambert Conformal map projection, run over three nested domains of 36 km - 12 km - 4 km with the innermost domain covering the YRD region (Fig. 17.1). The lateral and vertical boundary of WRF domain is 3 grids larger at each boundary and 13 layers more than the CAMx modelling domain respectively.

The simulation period is from first January to 31st March 2020 to cover the pre-lockdown stage (sixth to 24th January 2020); Level I response (24th January to 25th February 2020) and Level II response (25th February to 31st March 2020) periods. The first five days are model spin-up period. The provincial capital cities of Shanghai, Nanjing, Hangzhou, and Hefei are considered for comprehensive analysis, as shown in Fig. 17.1.

The most recent emission inventory developed by our group is utilised for the YRD region; the MEIC model (Multi-resolution Emission Inventory of China (http://www.meicmodel.org) for areas outside YRD (within China); and the MIX emission inventory (Li et al., 2017) for other Asian regions. In addition, a reduced emission inventory

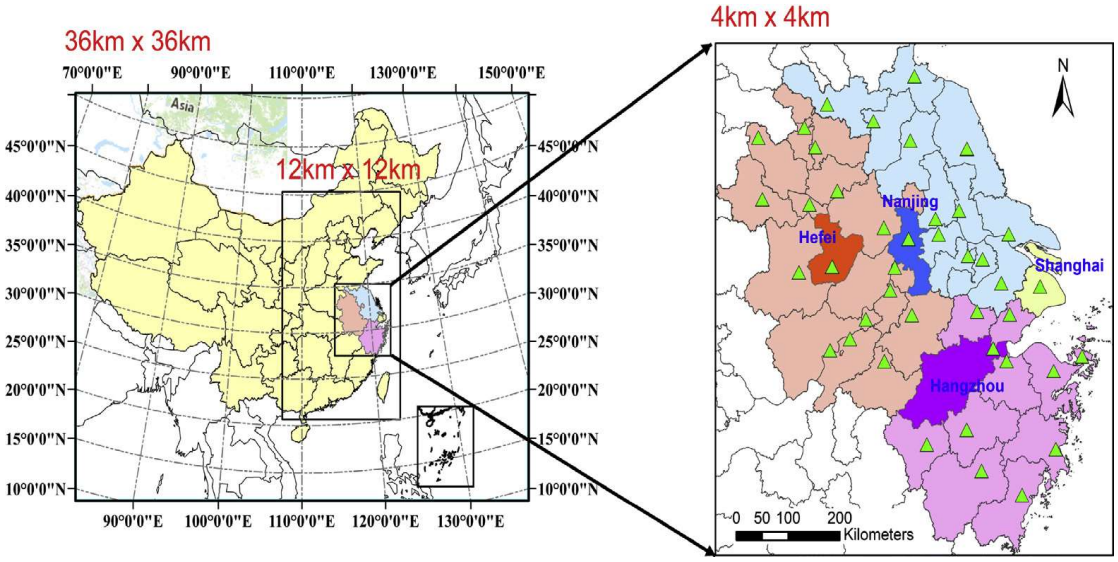

Fig. 17.1 Modelling domain and locations of the national observational sites (green triangle).

to account for the restricted human activities due to COVID-19 is developed based on reported activity data and best estimates. For emission reductions outside the YRD region during lockdown, we apply the reduction ratio used by Wang et al. (2020b). The Model of Emissions of Gases and Aerosols from Nature (MEGAN, v3.0, http://aqrp.ceer.utexas.edu/projects.cfm), the OCEANIC pre-processor developed by Ramboll (http://www.camx.com/download/support-software.aspx) and the Sparse Matrix Operator Kernel Emissions (SMOKE model, https://www.cmascenter.org/smoke) are used to prepare the gridded and speciated hourly biogenic, sea salt and anthropogenic emissions respectively.

17.2.3 Source contribution analysis

Potential source contribution factor (PSCF) analysis is applied to locate pollution sources using air mass trajectories (Duan et al., 2019; Liu et al., 2019). PSCF can be calculated for each 1° × 1° cell by dividing the number of trajectory endpoints corresponding to samples with factor scores or pollutant concentrations greater than specified values by the number of total endpoints in the cell (Hopke and Zeng, 1989). Since the deviation of PSCF results can increase with the raise of distance between cell and receptor, a weight factor, W_{ij}, is adopted in this study to lower the uncertainty of PSCF results (i.e. weighted PSCF, WPSCF); (Hopke and Zeng, 1989; Polissar et al., 1999; Zhang et al., 2019). Furthermore, the TrajStat modelling system is combined with the Global Data Assimilation System (GDAS) to analyse potential source contribution areas of $PM_{2.5}$ and show the air mass transport pathway within the YRD during different periods of COVID-19 respectively.

$$\mathrm{PSCF}_{ij} = m_{ij}/n_{ij} \tag{17.1}$$

$$\mathrm{WPSCF}_{ij} = \mathrm{PSCF}_{ij} \times W_{ij} \tag{17.2}$$

$$W_{ij} = \begin{cases} 1 & 2 \times Avg < n_{ij} \\ 0.7 & Avg < n_{ij} \le 2 \times Avg \\ 0.42 & 0.5 \times Avg < n_{ij} \le Avg \\ 0.05 & 0 < n_{ij} \le 0.5 \times Avg \end{cases} \tag{17.3}$$

Where n_{ij} and m_{ij} are the total number of back-trajectory segment endpoints that fall into the grid cell (i, j), during all days and in days when receptor concentrations were higher than the criteria value, respectively. A higher ratio of m_{ij} /n_{ij} indicates a higher probability of a particular grid through which a passing air mass would result in a higher receptor concentration. where Avg is the average number of trajectory segment endpoints in all cells.

17.2.4 Quantitative analysis of air quality changes during COVID-19

Air quality changes are analysed using the Brute Force Method (BFM) (Burr and Zhang, 2011), by running the model in its base state and then re-running it with adjusted

Table 17.2 Definition of CAMx PSAT groups.

No.	Source Category	Abbreviation	Emission source sector
1	Agriculture	AGR	Agriculture
2	Residential	RES	Cooking; Residential combustion
3	Dust	DST	Construction dust; Road dust
4	Industry	IND	Power plants; industrial boilers; industrial kilns; industrial processes
5	Biomass burning	BB	Biomass burning
6	Mobile	MOB	On-road vehicle exhaust; Non-road; Aircraft
7	Solvent use + storage	OTHER	Architectural coating; Household solvent usage; Hospital solvent usage; Gas station; Oil storage
8	Natural	NAT	Biogenic emissions; Sea-salt emissions

emissions. In this case, a *baseline-scenario* (C_b) utilises emissions from normal activities assuming no lockdown, while a *COVID-19 scenario* (C_s) is based on a reduced emission inventory. Through comparative analysis, a ratio of simulated concentrations between the two scenarios (i.e. relative improvement factor, *RF*), is combined with ground based observations (C_o) to assess air quality changes associated emission reductions due to lowered human activities during the lockdown (C_d), such that,

$$\mathrm{RF} = \frac{C_b - C_s}{C_b} \tag{17.4}$$

$$C_d = C_o.\mathrm{RF} \tag{17.5}$$

RF is calculated for Level I and Level II periods separately and applied at selected monitoring sites to reflect spatial variability of the changes of air quality associated with COVID-19 emission reductions.

The Particulate Source Apportionment Technology (PSAT) in CAMx is utilised to quantify the sectoral contributions to $PM_{2.5}$ (from eight source categories, Table 17.2). The differences in PSAT results under baseline and COVID-19 scenarios are used to quantify the contributions of $PM_{2.5}$ reductions associated with emissions reduction in each sector due to the lowered human activities.

17.2.5 Health impact assessment due to changes in air quality during COVID-19 lockdown

Premature mortality due to ambient $PM_{2.5}$ exposure is carried out based on a widely-used log-linear exposure-response function (Gao et al., 2016),

$$Y = \sum_k P \times (1 - e^{\beta_k (C - C_0)}) \times R_k \tag{17.6}$$

where Y is the number of premature deaths attributed to ambient $PM_{2.5}$ exposure due to five leading causes (k= 5) (i.e. cerebrovascular disease (stroke), ischemic heart disease

(IHD), chronic obstructive pulmonary disease (COPD), lung cancer (LC) for adults at least 25 years old, and acute lower respiratory infection (ALRI) for infants under 5 years of age). β is the cause-specific exposure-response coefficients and values reported from a meta-analysis study (Lu and Yao, 2015). Such that, a 10 μg m^{-3} increases in ambient $PM_{2.5}$, β is 0.63 percent for stoke and IHD (95 percent confidential interval (CI): 0.35 percent - 0.9 percent) and 0.75 percent for COPD, ALRI and LC (95 percent CI: 0.39 percent - 1.11 percent). R is the baseline incidence rate obtained from the Sixth National Population Census (http://www.stats.gov.cn/tjsj/pcsj/rkpc/6rp/indexch.htm), while the Global Burden of Diseases (GBD) estimates that stroke, IHD, COPD, LC, and ALRI contribute 20.2 percent, 16.7 percent, 9.2 percent, 6.4 percent and 1.7 percent of total deaths in China for 2017 respectively (https://vizhub.healthdata.org/gbd-compare/). Furthermore, P is the exposed population to $PM_{2.5}$ concentration (C) averaged during each period for each city in the YRD region. 25 μg m^{-3} is used as the threshold $PM_{2.5}$ concentration, C_0 , as per World Health Organization (WHO) air quality guidelines (World Health Organization, 2005).

The number of premature mortality is calculated using observed $PM_{2.5}$ concentrations during similar period of 2017–20 to show temporal trends over the past four years. The adjusted $PM_{2.5}$ concentrations calculated based on the RF method are used to calculate the number of premature mortality assuming no lockdown occurred. The differences between results obtained based on observed and adjusted $PM_{2.5}$ concentrations illustrate the health impacts due to changes in air quality during lockdown periods.

17.3 Results and discussion

17.3.1 Meteorological changes during the COVID-19

Generally during the COVID-19 period, there is no significant or observable change in the meteorological conditions during the period January to March from 2017 to 2020 in YRD region. Comparative analysis reveals that temperature, air pressure, and wind field in Shanghai, Hangzhou, Nanjing and Hefei match well with previous years, only that, the surface temperature and humidity in 2020 is slightly higher than previous years, falling well within normal statistical variations. Table 17.3

Table 17.3 Changes of meteorological parameters at typical cities in the YRD region (first January to 31st March).

	Temperature (°C)		Pressure (hPa)		Relative humidity (percent)		Wind Speed ($m \cdot s^{-1}$)	
	2017–19	2020	2017–19	2020	2017–19	2020	2017–19	2020
City	Avg±SD		Avg±SD		Avg±SD		Avg±SD	
Shanghai	7.9 ± 4.3	9.7 ± 4.2	1024.7 ± 5.8	1023.8 ± 5.6	74.8 ± 17.6	75.7 ± 16.8	4.8 ± 2.1	4.9 ± 2.0
Hangzhou	8.6 ± 5.1	10.2 ± 5.0	1024.2 ± 5.9	1023.4 ± 5.7	75.6 ± 19.4	76.4 ± 18.4	2.7 ± 1.4	2.5 ± 1.5
Nanjing	6.9 ± 5.7	8.5 ± 5.4	1024.6 ± 6.2	1023.7 ± 6.1	74.8 ± 20.6	78.3 ± 21.7	2.7 ± 1.6	2.6 ± 1.6
Hefei	6.8 ± 6.0	8.1 ± 5.8	1024.2 ± 6.4	1022.7 ± 5.8	74.1 ± 20.5	79.2 ± 21.6	3.0 ± 1.6	3.1 ± 1.6

17.3.2 Air quality changes due to COVID-19 lockdown

17.3.2.1 Observed air quality changes during the COVID-19 lockdown

In Fig. 17.2, the concentration of $PM_{2.5}$ before and during the lockdown exhibit blanket reduction across the YRD region. It is evident that substantial decrease in $PM_{2.5}$ is mostly confined in the highly urbanised central areas ofYRD where vehicular traffic is usually high. Generally, the level of $PM_{2.5}$ in YRD during the lockdown

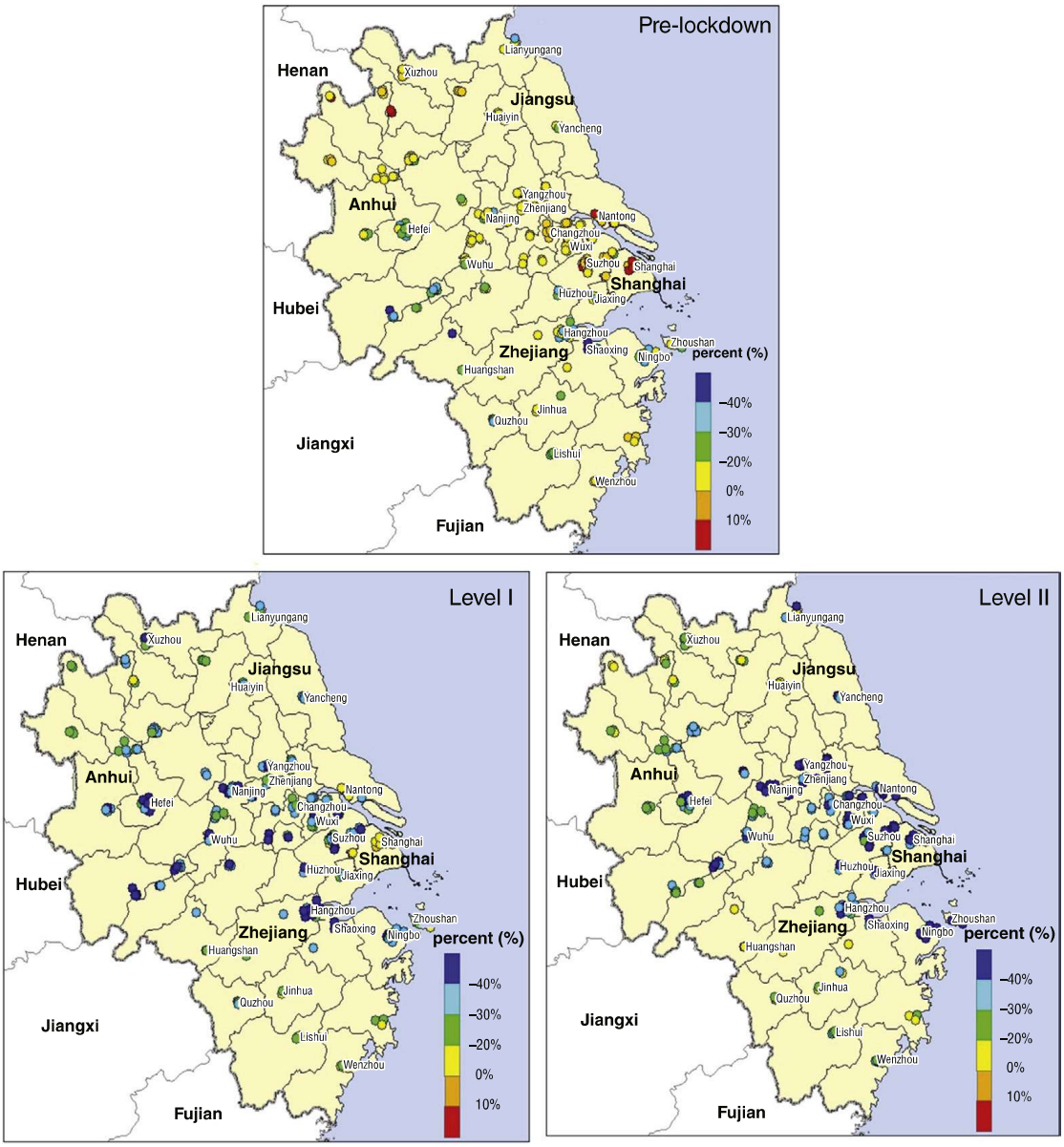

Fig. 17.2 (Top) relative changes of $PM_{2.5}$ before lockdown and during lockdown; (bottom left) $PM_{2.5}$ concentrations during lockdown period and (bottom right) adjusted $PM_{2.5}$ concentrations in the YRD.

period can be considered to be at good air quality level based on internationally recognised standards.

Furthermore and unsurprisingly, other air pollutants also reveal drastic reduction during the COVID-19 lockdown period in YRD (Fig. 17.3). For instance, the average concentrations of criteria pollutants (PM_{10}, CO, NO_2 and SO_2) in the YRD region decreased substantially in 2020, except the rebounding of O_3-8 h compared to similar period in 2017–19. In fact, a double-digits change was realised during Level I and Level II response periods (Table 17.4). From these results, it is clear that the lockdown during COVID-19 period produced the conspicuous air pollution reduction in the YRD region.

17.3.2.2 Simulation of air quality changes during the COVID-19 lockdown

If no lockdown had occurred (i.e. emissions had been at baseline level), $PM_{2.5}$ concentrations in Shanghai and the entire northern YRD are estimated to be between 50–100 μg m^{-3}, which is about 60 percent higher than lockdown values.

Detailed scrutiny (Table 17.5) reveals that, during Level I response period, Zhejiang, Anhui and Jiangsu experienced a more pronounced air quality improvement compared to Shanghai. This signifies the slightly different level of implementation of lockdown from each province.

Subsequently, during Level II, it is also apparent that the extended Level I response in Shanghai, as mentioned earlier, produced a much higher improvement. It is understandable that the prominent drop of NO_2 (high *RF*) is directly related to the sharp decrease of VKT as a result of the lockdown. Similarly, the sharp decreases in SO_2, particularly in Anhui, Zhejiang and Jiangsu, where industries are concentrated, are linked to the stoppage of industrial activities, as well as small and medium enterprises during the lockdown period. In contrast, significant ozone increase is seen in the areas with higher NO_2 and $PM_{2.5}$ decrease. This phenomenon is attributed to a weakened ozone titration due to the sharp drop of NO_x emissions during the lockdown. Recent studies also suggest that a decrease in $PM_{2.5}$ and its chemistry, makes ozone less sensitive to NO_x controls, because ideally $PM_{2.5}$ acts as a sink for NO_x radicals that would otherwise have produced ozone. Therefore, policies focused on reducing the regional atmospheric oxidation capacity are urgently needed to tackle the increasing ozone phenomenon in the YRD region, especially with regarding to its interconnectivity with $PM_{2.5}$ and NO_x.

17.3.3 Clustering analysis and potential source contributions

To study the air mass trajectories and source characteristics of $PM_{2.5}$ in the YRD, a PSCF threshold of 75 μg m^{-3} is set to make it consistent with the daily average standard.

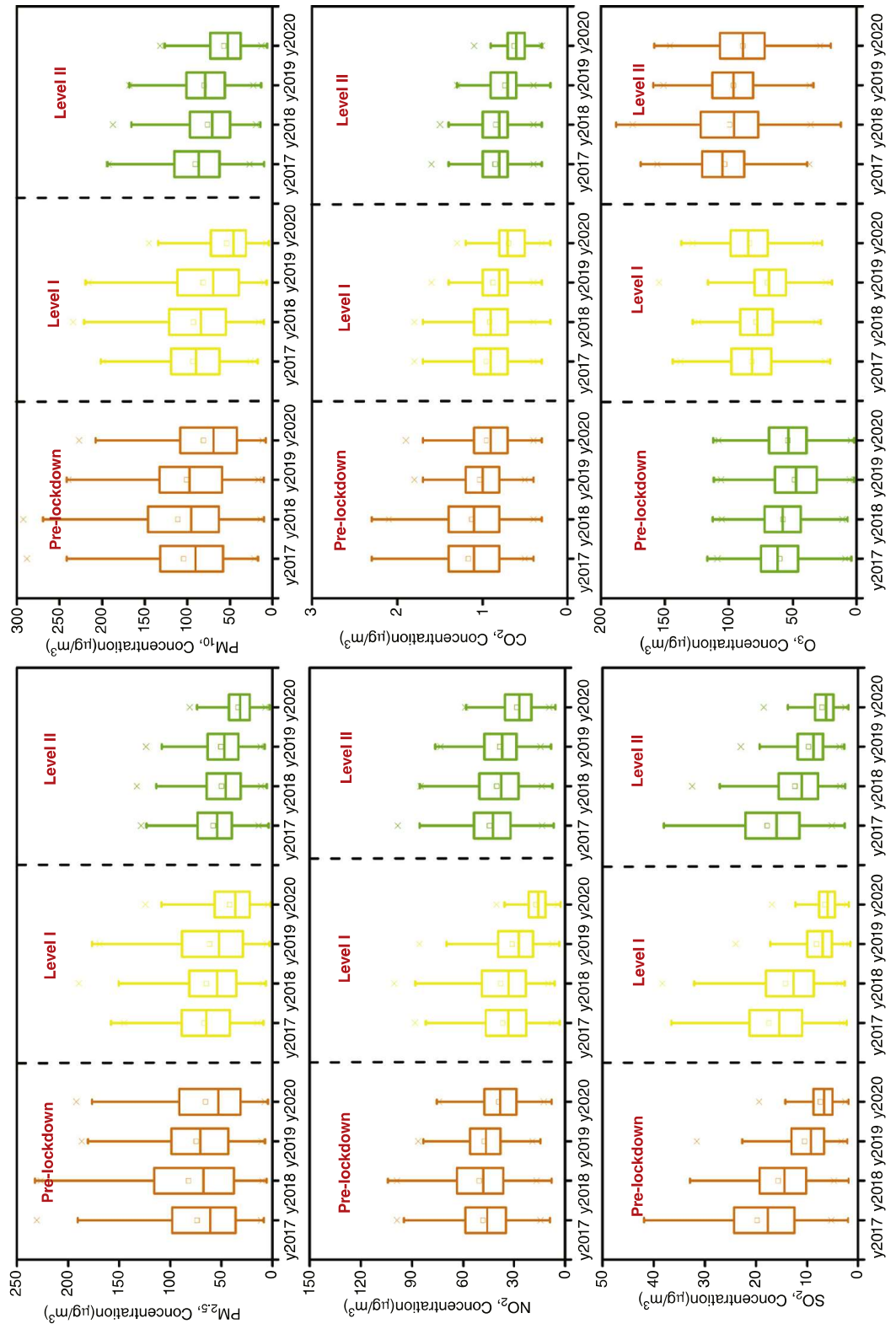

Fig. 17.3 Yearly changes of $PM_{2.5}$, PM10, CO, NO_2, SO_2 and O_3-8h in 41 cities in the YRD (first January - 31st March).

Table 17.4 Comparison of various pollutants in 2019 and 2020 in YRD (first January - 31st March).

	Pre-lockdown			Level I Response Period			Level II Response Period		
Pollutants	**2019**	**2020**	**Changing rate**	**2019**	**2020**	**Changing rate**	**2019**	**2020**	**Changing rate**
$PM_{2.5}$	75	66	−12.3 percent	62	42	−31.8 percent	51	34	−33.2 percent
PM_{10}	101	81	−19.6 percent	81	54	−33.7 percent	81	57	−29.0 percent
CO	1.0	1.0	−7.8 percent	0.9	0.7	−20.9 percent	0.7	0.6	−14.7 percent
NO_2	48	39	−18.5 percent	31	17	−45.1 percent	38	28	−25.9 percent
SO_2	11	7	−29.3 percent	8	7	−20.4 percent	10	7	−27.2 percent
O_3-8h	49	54	10.4 percent	70	84	20.5 percent	96	89	−7.6 percent

Table 17.5 Changes of key pollutants' concentrations in key cities of YRD region during 2020 COVID-19 lockdown.

		Level I			Level II		
Province		**Observed (μg m^{-3})**	**Relative Improvement Factor (RF)**	**Changes due to lockdown (μg m^{-3})**	**Observed (μg m^{-3})**	**Relative Improvement Factor (RF)**	**Changes due to lockdown (μg m^{-3})**
Shanghai	$PM_{2.5}$	36.5	−40.9 percent	−14.9	26.9	−34.9 percent	−9.4
	NO_2	27.2	−59.1 percent	−16.1	32.2	−52.8 percent	−17.0
	SO_2	6.1	−24.6 percent	−1.5	6.3	−17.6 percent	−1.1
	O_3	69.1	24.2 percent	16.7	75.6	16.8 percent	12.7
Anhui	$PM_{2.5}$	50.2	−35.5 percent	−18.1	40.2	−21.6 percent	−8.7
	NO_2	18.4	−55.6 percent	−10.0	27.6	−23.4 percent	−6.3
	SO_2	7.6	−27.3 percent	−2.1	8.0	−18.0 percent	−1.4
	O_3	62.4	9.20 percent	5.9	61.9	1.0 percent	0.7
Zhejiang	$PM_{2.5}$	26.0	−38.0 percent	−9.9	23.5	−27.6 percent	−6.5
	NO_2	13.1	−51.2 percent	−6.6	29.1	−28.2 percent	−8.0
	SO_2	5.1	−32.0 percent	−1.6	5.9	−18.8 percent	−1.1
	O_3	65.6	2.9 percent	2.1	59.3	0.8 percent	0.6
Jiangsu	$PM_{2.5}$	46.2	−40.4 percent	−18.7	35.2	−24.5 percent	−8.7
	NO_2	18.0	−51.4 percent	−9.2	28.5	−25.3 percent	−7.0
	SO_2	6.4	−28.8 percent	−1.9	7.1	−16.7 percent	−1.2
	O_3	64.4	8.0 percent	5.1	68.1	3.2 percent	2.2

From the PSCF results (Fig. 17.4), dark grid colours represent greater contribution of the potential source area to the concentration of $PM_{2.5}$ in Shanghai. From the Figure, it can be seen that $PM_{2.5}$ in Shanghai is contributed by a wide and complex sources of pollution. This includes the neighbouring provinces and also other areas such as

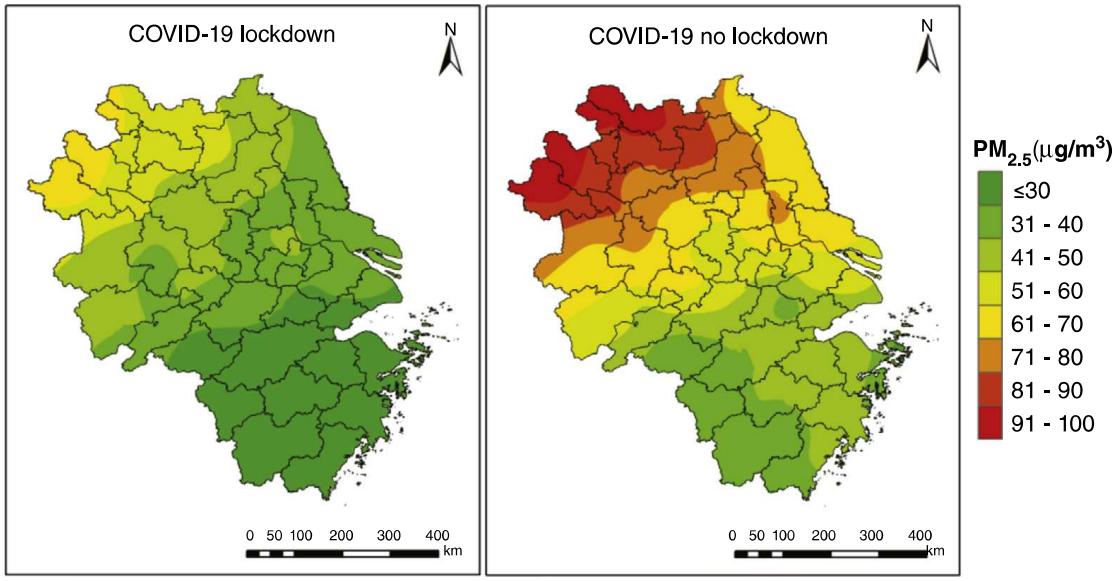

Fig. 17.4 Concentration of $PM_{2.5}$ during lockdown period and (left) and adjusted $PM_{2.5}$ concentrations in the YRD.

Shandong, Henan, Shanxi, Hebei, Jiangxi, Hunan, Beijing, Tianjin, Hebei, and other regions. Clearly, a major fraction of concentration of $PM_{2.5}$ in Shanghai comes from long-range transport, as in Fig. 17.5.

The air mass trajectories during pre-lockdown period mainly originate from the Northern Mongolia region and as far as Siberia. These air masses carry primary and secondary air pollutants through long distances and reach the YRD region via Beijing, Tianjin and the Yellow Sea region. During Level I response, local sources and adjacent areas in the North and Northwest of Shanghai (i.e. Xuzhou-Suzhou-Wuxi-Changzhou-Nantong area) were the main potential impact sources with WPSCF is above 0.6. Moreover, the regional potential sources (WPSCF > 0.5) and the polluted air mass from the north landed on the eastern coastal area after detouring at the sea (WPSCF of 0.3–0.4), thus impacting the concentration of $PM_{2.5}$ in Shanghai.

During Level II period, $PM_{2.5}$ in Shanghai is mainly affected by the contribution of surrounding cities within YRD, particularly the southwestern city of Huzhou with a WPSCF above 0.6 (Fig. 17.4). In addition, YRD region is greatly affected by the monsoon climate owing to its location. Usually during March Shanghai receives more southerly winds (i.e. southeast and southwesterly winds), which causes polluted air masses. Besides, after Level II response was effected, industries resumed production, and economic activities brought more anthropogenic pollution sources which eventually impacted $PM_{2.5}$ in Shanghai. In conclusion, the PSCF results reveal an intricate and complex wintertime pollution sources of $PM_{2.5}$ in the YRD region, especially in Shanghai that require large-scale regional joint-control strategies.

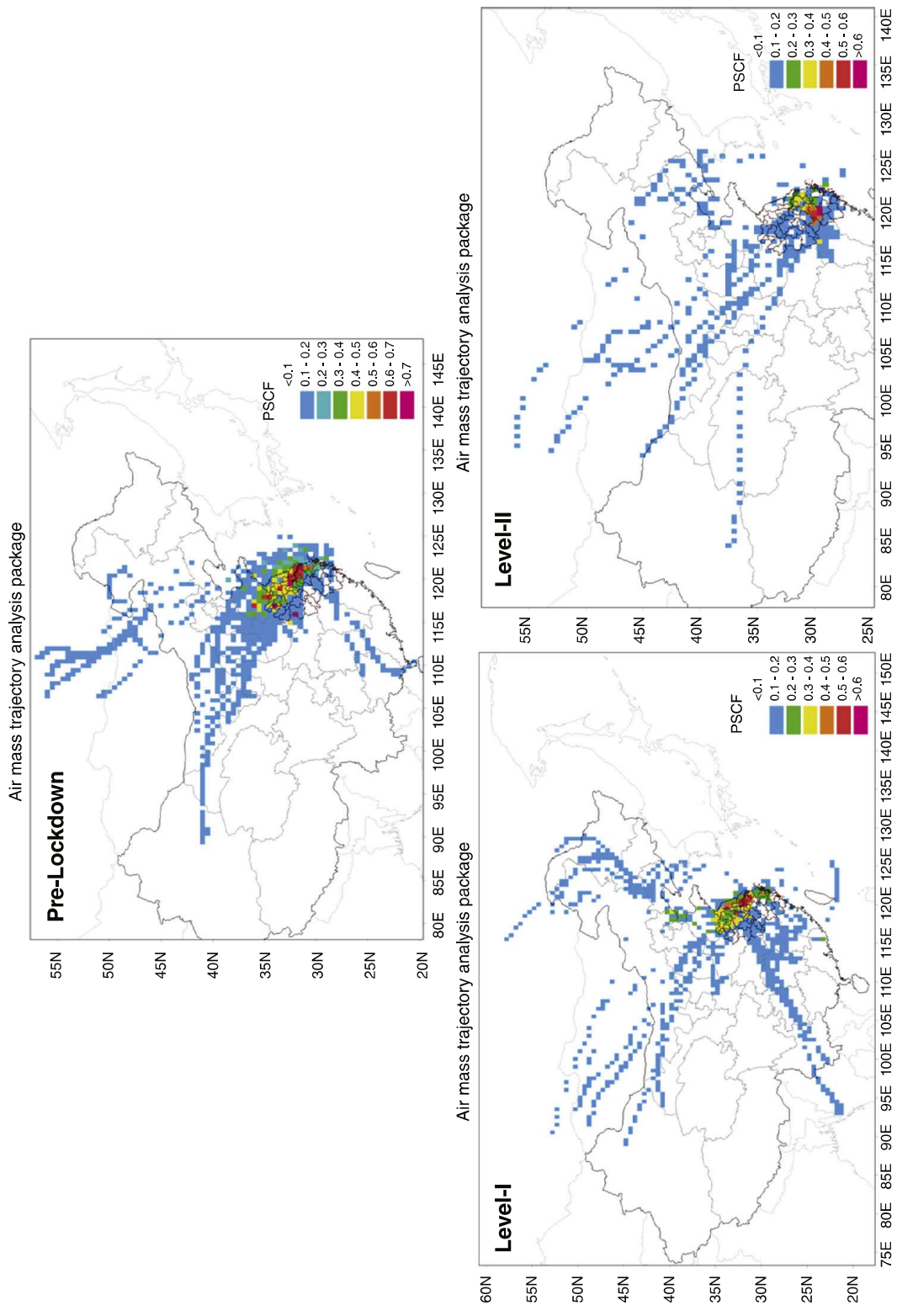

Fig. 17.5 PM2.5 potential source regions: air mass trajectory analysis during COVID-19 period in Shanghai.

17.3.3.1 Source apportionment of $PM_{2.5}$ during COVID-19 lockdown

Before and during the COVID-19 period, industrial and residential contributions to $PM_{2.5}$ were significant. This is the case because according to the industrial production data published by the bureau of statistics in the provinces of YRD, the manufacturing sector did not actually show major slowdown. The production of iron and other non-ferrous materials, medical and pharmaceuticals remained roughly constant. However, the report noted the petrochemical industry, construction industry and facility manufacturing were strongly affected and hampered by both the upstream and downstream chain. Fig. 17.6

It is also worth noting that the promulgation of Level I response coincided with the Chinese New Year holidays, starting 25th January 2020. Therefore, the lockdown restrictions confined most people within their homes leading to the increase in residential emissions. In contrast, the contribution of dust (DST) and mobile (MOB) emissions to $PM_{2.5}$ show substantial reduction. This is attributed to the shutdown of the construction sector and the restriction of travel during the lockdown. Data published by the bureaux of statistics of Anhui and Zhejiang provinces show a drop of about 50 percent in passenger traffic in both provinces between January-February 2020 compared to the same period in 2019. Traffic flow monitoring data from Bengbu and Changzhou cities show a 75 percent and 50 percent decline during Level I and Level II respectively, compared to pre-epidemic period. As to the total departures from China's 25 busiest airports (Flightradar 24, https://www.flightradar24.com/), the decline during Level I and Level II is 80 percent and 60 percent, respectively.

17.3.4 Impact of air quality changes on health during COVID-19 lockdown

17.3.4.1 Premature mortality attributable to short-term $PM_{2.5}$ exposure

As mentioned before, ambient $PM_{2.5}$ exposure leads to higher mortality in infants (< 5 years) because of ALRI and in adults (≥ 25 years) due to stroke, IHD, COPD and LC. Therefore, premature mortality over the YRD region is calculated based on the health impact function (Eq. (17.6) during pre-lockdown, Level I, and Level II period of 2017–20.

In 2020 during the pre-lockdown period, the total premature mortality attributed to $PM_{2.5}$ exposure is 36.4 thousand (95 percent CI: 30.4–38.8 thousand) in the YRD region (Fig. 17.7). The previous years (i.e. 2017–19) show relatively consistent results. It is noted that stroke and IHD account for over 70 percent of total $PM_{2.5}$-related premature death during the pre-lockdown period. During Level I and Level II response periods, a clear contrast is visible between 2017–19 when compared with 2020. Although

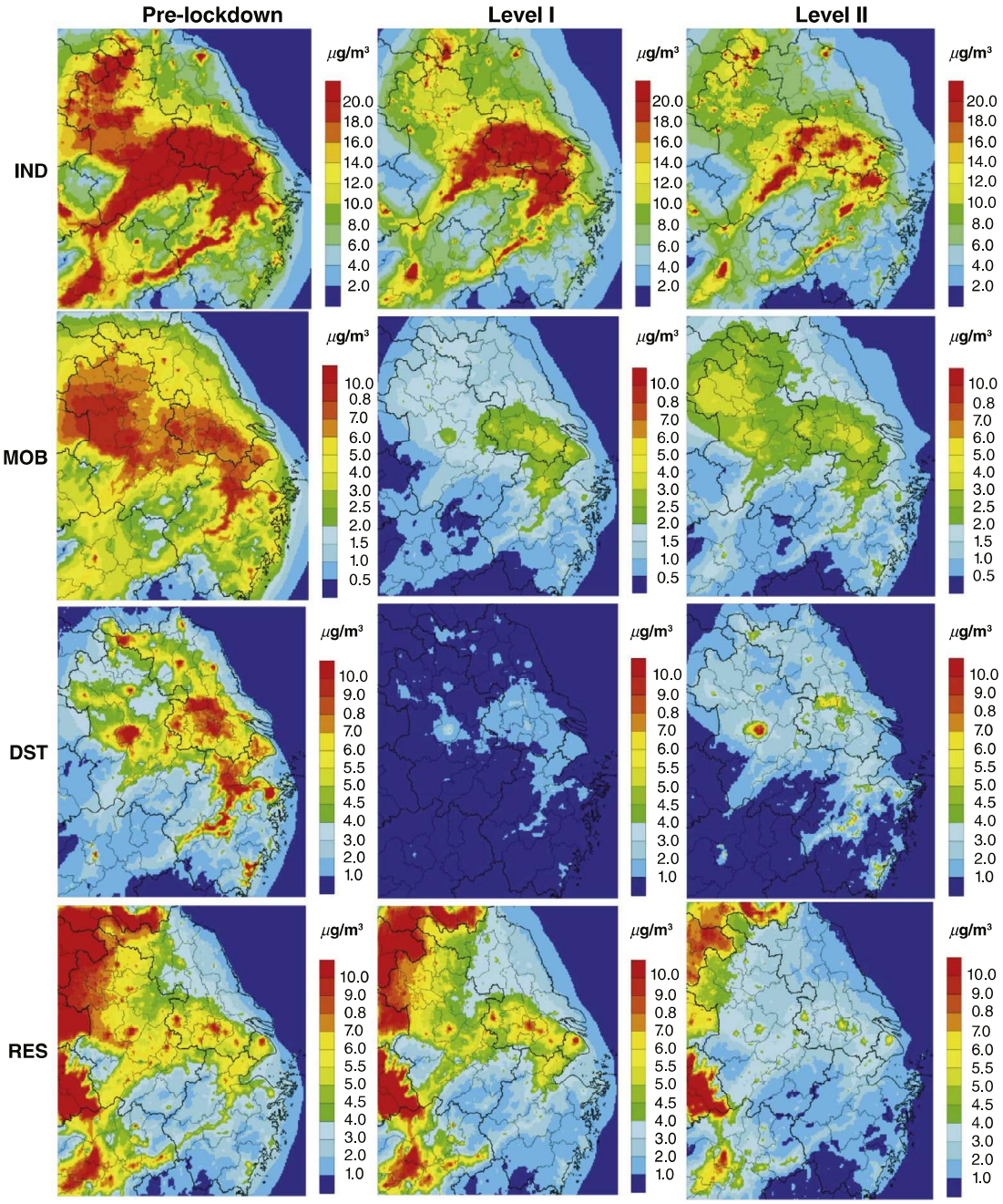

Fig. 17.6 Sectoral contributions to PM2.5 during pre-lockdown, Level I and Level II response periods in YRD.

the results of 2017–19 exhibit slight fluctuations, a clear contrast is visible in the results of 2020. Therefore, the significant reduction in premature mortality during lockdown periods (Level *I* + Level II), indicate clearly the substantial health benefits associated with lowered $PM_{2.5}$ concentrations due to the COVID-19 lockdown.

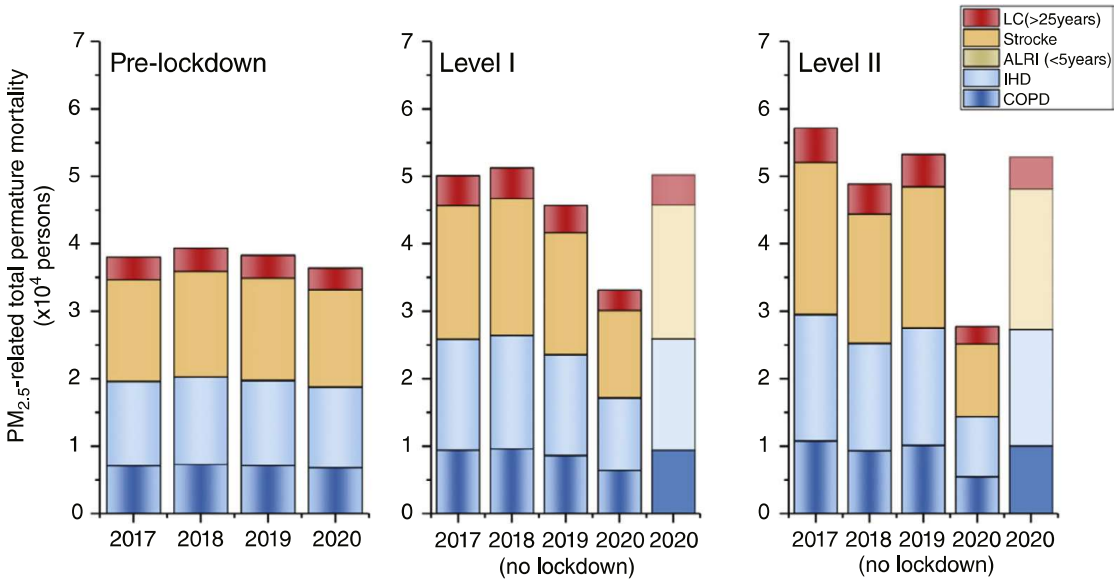

Fig. 17.7 ***Premature mortality due to LC, stroke, ALRI, IHD, COPD during pre-lockdown, Level I and Level II periods of 2017–20.*** Estimated premature mortality with the assumption of no-lockdown is also shown for Level I and Level II.

17.3.4.2 Avoided premature mortality due to relative improvement of $PM_{2.5}$ during COVID-19 lockdown

The potential health benefits due to lockdown are estimated as the differences of premature mortality calculated with observed $PM_{2.5}$ concentrations and the simulated 'no lockdown' concentrations. The number of avoided premature death for different cities depends on the base population and the changes in $PM_{2.5}$ concentrations due to lockdown. During Level I period, the top five cities with largest avoided premature death are Shanghai (1932), Wenzhou (1124), Suzhou (Jiangsu province; 1118), Ningbo (934), and Hangzhou (934). During Level II period, the top five cities with largest avoided premature death are Shanghai (3502), Wenzhou (1628), Suzhou (Jiangsu province; 1542), Nantong (1270), and Nanjing (1227). This is not to imply that COVID-19 of any positive consequences, but more about to initiate a discussion with evidence that air pollution has tremendous health effects. Fig. 17.8

17.4 Conclusions

COVID-19 control period was characterised by major reduction of human activities which led to significant reduction in primary pollutants like $PM_{2.5}$, NO_x, SO_2 and VOCs. However, it was discovered that during the period O_3 rebounded. This indicates the complexity in the co-control of $PM_{2.5}$ and O_3, especially with regard to the titration effect with NOx. Therefore, more stringent measures such as adjustment of the energy and industrial structure; more stringent and wider regional joint-control to achieve a better air quality.

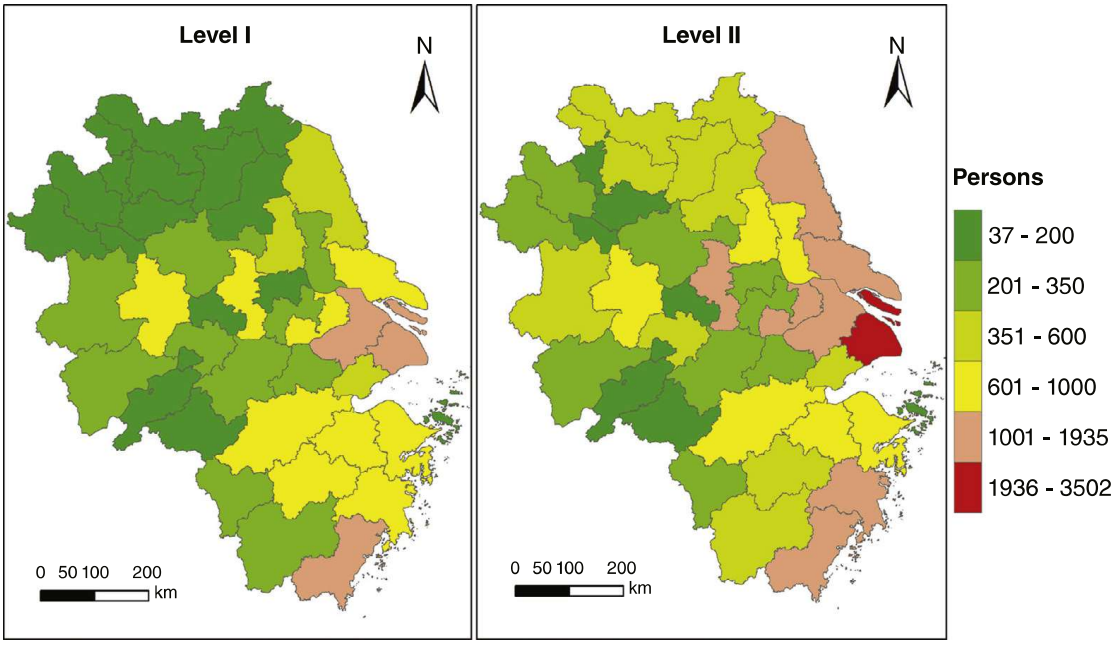

Fig. 17.8 Spatial distribution of city-level total avoided premature death during COVID-19 lockdown in YRD.

It is also worth to note that, the COVID-19 pandemic continues run havoc globally. For that reason, our results of this study has no intention to indicate that pandemics bring a positive effect on health, rather, the COVID-19 lockdown in YRD provided a good opportunity to reveal the health impacts related to improved air quality. In fact, our results strongly reinforce our knowledge on detrimental health effects that $PM_{2.5}$ has. Moreover, it is now evident that substantial health benefits can be achieved with reduced $PM_{2.5}$ concentrations as a result of emission controls. However, although $PM_{2.5}$ concentration decreased substantially during lockdown period, there is evidence of high concentrations of residual $PM_{2.5}$ that exceed the WHO standards. Therefore, continuous efforts are needed to reduce emissions in the long term and through the most cost-effective ways in order to protect public health.

References

Burr, M.J., Zhang, Y., 2011. Source apportionment of fine particulate matter over the Eastern U.S. Part I: source sensitivity simulations using CMAQ with the Brute Force method. Atmos Pollut Res 2, 300–317, https://doi.org/10.5094/apr.2011.036.

Chang, J.S., Brost, R.A., Isaksen, I.S.A., Madronich, S., Middleton, P., Stockwell, W.R., et al., 1987. A 3-dimensional eulerian acid deposition model physical concepts and formulation. J.of Geophysical Res.-Atmospheres 92, 14681–14700, https://doi.org/10.1029/JD092iD12p14681.

Chou, M.D., Lee, K.T., Tsay, S.C., Fu, Q., 1999. Parameterization for cloud longwave scattering for use in atmospheric models. J Clim 12, 159–169, https://doi.org/10.1175/1520-0442-12.1.159.

Duan, S.G., Jiang, N., Yang, L.M., Zhang, R.-.Q., 2019. Transport pathways and potential sources of $PM_{2.5}$ during the Winter in Zhengzhou. Environ. Sci. 40, 86–93, https://doi.org/10.13227/j.hjkx.201805187.

Ek, M.B., Mitchell, K.E., Lin, Y., Rogers, E., Grunmann, P., Koren, V., et al., 2003. Implementation of Noah land surface model advances in the National Centers for Environmental Prediction operational mesoscale Eta model. J. of Geophysical Res.-Atmospheres 108 (16), https://doi.org/10.1029/2002jd003296.

Gao, J., Yuan, Z., Liu, X., Xia, X., Huang, X., Dong, Z., 2016. Improving air pollution control policy in China—A perspective based on cost–benefit analysis. Sci. Total Environ. 543, 307–314.

Hong, S.-.Y., Noh, Y., Dudhia, J., 2006. A new vertical diffusion package with an explicit treatment of entrainment processes. Mon. Weather Rev. 134, 2318–2341, https://doi.org/10.1175/mwr3199.1.

Hopke, P.K., Zeng, Y., 1989. A study of the sources of acid precipitation in Ontario, Canada. Atmos. Environ. 23, 1499–1509, https://doi.org/10.1016/0004-6981(89)90409-5.

Huang, L., An, J., Koo, B., Yarwood, G., Yan, R., Wang, Y., et al., 2019. Sulfate formation during heavy winter haze events and the potential contribution from heterogeneous SO_2 + NO_2 reactions in the Yangtze River Delta region. China. Atmos. Chem. Phy. 19, 14311–14328, https://doi.org/10.5194/acp-19-14311-2019.

Li, L., An, J., Zhou, M., Qiao, L., Zhu, S., Yang, R., et al., 2018. An integrated source apportionment methodology and its application over the Yangtze River Delta Region. China. Environ. Sci. & Tech. 52, 14216–14227, https://doi.org/10.1021/acs.est.8b01211.

Li, L., Zhu, S., An, J., Zhou, M., Wang, H., Yan, R., et al., 2019. Evaluation of the effect of regional joint-control measures on changing photochemical transformation: a comprehensive study of the optimization scenario analysis. Atmos. Chem. Phys. 19, 9037–9060, https://doi.org/10.5194/acp-19-9037-2019.

Li M., Zhang Q., Kurokawa J-i, Woo J.-.H., He K., Lu Z., et al., 2017. MIX: a mosaic Asian anthropogenic emission inventory under the international collaboration framework of the MICS-Asia and HTAP. Atmos. Chem. Phys. 17, 935-963, https://doi.org/10.5194/acp-17-935-2017.

Lin, Y.L., Farley, R.D., Orville, H.D., 1983. Bulk parameterization of the snow field in a cloud model. J. of climate and appl. meteorol. 22, 1065–1092, https://doi.org/10.1175/1520-0450 (1983)022<1065:bpotsf>2.0.co;2.

Liu, T., Wang, X.J., Chen, Q., Wen, J., Huang, B., Zhu, H.X., et al., 2019. Pollution characteristics and source apportionment of ambient $PM_{2.5}$ during four seasons in Yantai City. Environ. Sci. 40, 1082–1090, https://doi.org/10.13227/j.hjkx.201807252.

Lu, M., Yao, W.Z., 2015. Asthma and chronic obstructive pulmonary disease overlap syndrome: An update. J. Transl. Int. Med. 3(4), 144.

Kain, J.S., Fritsch, J.M., 1993. Convective Parameterization for Mesoscale Models: The Kain-Fritsch Scheme. In: Emanuel K.A., Raymond D.J. (Eds.), The Representation of Cumulus Convection in Numerical Models., Meteorological Monographs. American Meteorological Society, Boston, MA, https://doi.org/10.1007/978-1-935704-13-3_16.

Mlawer, E.J., Taubman, S.J., Brown, P.D., Iacono, M.J., Clough, S.A., 1997. Radiative transfer for inhomogeneous atmospheres: RRTM, a validated correlated-k model for the longwave. J.Geophy. Res.-Atmospheres 102, 16663–16682, https://doi.org/10.1029/97jd00237.

NASA, 2020. The earth observatory. Retrieved from https://earthobservatory.nasa.gov/images/146362/airborne-nitrogen-dioxide-plummets-over-china.

Polissar, A.V., Hopke, P.K., Paatero, P., Kaufmann, Y.J., Hall, D.K., Bodhaine, B.A., et al., 1999. The aerosol at Barrow, Alaska: long-term trends and source locations. Atmos. Environ. 33, 2441–2458, https://doi.org/10.1016/s1352-2310(98)00423-3.

Tian, H., Liu, Y., Li, Y., Wu, C.H., Chen, B., Kraemer, M.U.G., et al., 2020. An investigation of transmission control measures during the first 50 days of the COVID-19 epidemic in China. Science (New York, N.Y.), https://doi.org/10.1126/science.abb6105.

Wang, C., Horby, P.W., Hayden, F.G., Gao, G.F., 2020a. A novel coronavirus outbreak of global health concern. Lancet 395, 470–473, https://doi.org/10.1016/s0140-6736(20)30185-9.

Wang, P., Chen, K., Zhu, S., Wang, P., Zhang, H., 2020b. Severe air pollution events not avoided by reduced anthropogenic activities during COVID-19 outbreak. Resour. Conserv. Recycl. 158, 104814, https://doi.org/10.1016/j.resconrec.2020.104814.

World Health Organization, 2005. Pocket book of hospital care for children: guidelines for the management of common illnesses with limited resources. World Health Organization.
Yarwood, G., et al., 2010. Updates to the carbon bond mechanism for version 6(CB6), Presented at the 9th Annual CMAS Conference. Chapel Hill October.
Zhang, H.-Y., Cheng, S.-Y., Yao, S., Wang, X.-Q., Zhang, J.-F., 2019. Pollution characteristics and regional transport of atmospheric particulate matter in Beijing from October to November 2016. Environ. Sci. 40, 1999–2009, https://doi.org/10.13227/j.hjkx.201810228.